

## Supplementary Information

### Single-Molecule Contact Switching via Electro-inductive Effects

*Ya-Li Zhang,<sup>†,a</sup> Tian-Hang Bai,<sup>†,a</sup> Jing-Tao Ye,<sup>†,a</sup> Li-Na Luo,<sup>a</sup> Qiang Wan,<sup>\*,a</sup> Ju-Fang  
Zheng,<sup>a</sup> Yong Shao,<sup>a</sup> Ya-Hao Wang,<sup>\*,a</sup> Xiao-Shun Zhou<sup>\*,a</sup>*

<sup>a</sup>Key Laboratory of the Ministry of Education for Advanced Catalysis Materials,  
Institute of Physical Chemistry, College of Chemistry and Materials Science, Zhejiang  
Normal University, Jinhua 321004, P. R. China

E-mail: xszhou@zjnu.edu.cn; yahaowang@zjnu.edu.cn; qiangwan@zjnu.edu.cn

<sup>†</sup> These authors contributed equally

# 1. Experimental details

## Conductance measurements.

The STM-BJ technique is used to construct the molecular junction and measure their conductance. These measurements are carried out at a custom-modified Nanoscope IIIa STM (Veeco, USA).<sup>1-3</sup> The plane on an Au(111) bead substrates and the mechanically cut Au STM tip (a diameter of 0.25 mm with 99.999% purity from Alfa Aesar) are used as working electrodes. Prior to each experiment, the substrates undergo electrochemical polishing and flame annealing to ensure cleanliness and atomically flat surfaces. To minimize leakage current, the Au STM tips are insulated with wax.

The procedure of STM-BJ method can be briefly described as follows: Firstly, the STM tip is driven toward the substrate to a preset current value (50 nA) via piezoelectric control. Then an external pulse voltage is applied on z-piezo to bring STM tip into the substrate surface to ensure tip contact with the substrate. Then the tip is pulled away from the substrate at a constant speed of 20 nm/s. During the process, molecular junctions can be formed. Meanwhile, the current of the tip is recorded at a sampling rate of 20 kHz. Thousands of tip current-displacement curves are collected to construct the conductance histogram without data selection. The conductance measurement is carried out at a bias voltage of -50 mV.

The conductance measurements at different  $E_{\text{substrate}}$  were carried out at a four-electrode electrochemical system, the Pt ring and Pt wire were used as counter electrode and reference electrode respectively.

## Electrochemical Raman measurements.

According to previous reports,<sup>4, 5</sup> the 55 nm Au nanospheres were synthesized according to the following procedure: 1.4 mL of sodium citrate solution (1 wt%) was quickly added into 200 mL of boiling  $\text{HAuCl}_4$  solution (0.01 wt%). Then the mixture was refluxed for 20 min to obtain the spherical nanoparticles with a diameter ca. 55 nm. Finally, the Au colloidal solution was cooled to room temperature in ambient atmosphere for the preparation of Au @  $\text{SiO}_2$  nanoparticles.

The 55 nm Au @ ca. 2 nm  $\text{SiO}_2$  nanoparticles were prepared according to following procedures: 0.4 mL of (3-Aminopropyl) trimethoxysilane solution (1 mM) was dropwise added

into 30 mL of the as-prepared Au solution under stirring at room temperature. Next, 3.2 mL of sodium silicate solution (0.54 wt%) was quickly added to the solution, then transferred to 99°C water bath and stirred for 30 min. Finally, pipette 1.5 mL of the hot solution into a centrifuge tube and immediately immerse it in ice bath to stop the reaction. The solution was centrifuged at 4500 rpm and washed twice with Milli-Q water for the Raman measurements

Raman experiments were carried out on a confocal microscope Raman system (Renishaw InVia). The excitation wavelength was 633 nm, and a 50× microscope objective with a numerical aperture of 0.55 was used in all Raman measurements. The as-prepared 55 nm Au @ ca. 2 nm SiO<sub>2</sub> nanoparticles were dropped on the Au(111) electrode as Raman-signal amplifiers. A home-made Raman cell with potential control at an CHI660E potentiostat was used for in situ electrochemical Raman experiments.

#### **I-V measurements.**

The procedure of I-V measurements performed in electrochemical environment (0.1 mM BPB + 30 mM LiBF<sub>4</sub> in PC) is described as follows: First, a series of images of the Au(111) surface are captured. Once almost no drift is detected, the imaging size is adjusted to zero, and the STM feedback is subsequently disabled. Second the encapsulated Au tip is driven toward the substrate to a preset current value (50 nA) via piezoelectric control. Then an external pulse voltage is applied on z-piezo to bring STM tip 1 nm into the substrate surface to ensure tip contact with the substrate. Third, the tip is withdrawn to form single-molecule junction. When detecting the tip current reaches the product of the single-molecule conductance (obtained from STM-BJ experiments) and the bias voltage, indicating the formation of a single-molecule junction. The tip will be suspended over the substrate. Then the  $E_{\text{substrate}}$  is sweeping from 0 to -0.6 V with a constant bias voltage of -50 mV between substrate and tip, meanwhile tip current is recorded to obtain the I-V curves.

#### **I-t measurements.**

Firstly, the STM tip is stabilized over the substrate at a preset tunneling current of 0.19 nA with a bias voltage of -50 mV for at least an hour. Then the STM feedback loop is turned off, meanwhile the tip current- time curve is recorded for few seconds. When molecules are trapped in to tip-substrate nanogap and form a molecular junction, a sudden current increase (current blinking) would be observed.

## Computational methods.

The geometric optimizations, Raman and UV-vis spectra for molecules BPB and  $\text{LiBF}_4$  were performed at the B3LYP/6-311G(d, p) level by GAUSSIAN09.<sup>6</sup> All spin-polarized DFT calculations for the molecules on Au(111) were carried out by using Vienna ab initio Simulation Package (VASP).<sup>7</sup> The projected-augmented wave (PAW) pseudopotentials were utilized to describe the core electrons,<sup>8</sup> while valence electrons were treated by plane waves with a kinetic energy cutoff of 500 eV. The exchange-correlation potential was treated within the generalized gradient approximation according to Perdew-Burke-Ernzerhof (PBE) functional.<sup>9</sup> The DFT-D3 method of Grimme with the zero-damping function was adopted for vdW-dispersion energy correction.<sup>10</sup> The convergence criteria of energy and force were set to  $1 \times 10^{-5}$  eV and  $0.01 \text{ eV} \cdot \text{\AA}^{-1}$ , respectively. A  $3 \times 3$  supercell of Au(111) was used to model the Au electrode, consisting of 4 atomic layers of Au, with a vacuum space larger than  $15 \text{ \AA}$  along the z direction was applied to prevent the interaction between periodic boundaries. The bottom two layers were fixed during the structural optimization while the others were fully relaxed. The k-point mesh in Monkhorst-Pack scheme was set to  $3 \times 3 \times 1$  and  $5 \times 5 \times 1$  for geometric optimization and electronic structure, respectively.<sup>11</sup>

The binding energy ( $E_b$ ) for  $\text{BF}_3$  at the N site of \*BPB was calculated using the following equation:

$$E_b = E(\text{Au-BPB-BF}_3) - E(\text{Au-BPB}) - E(\text{BF}_3)$$

where the  $E(\text{Au-BPB-BF}_3)$ ,  $E(\text{Au-BPB})$  and  $E(\text{BF}_3)$  represent the energies of BPB- $\text{BF}_3$  on Au(111), BPB on Au(111), and the isolated  $\text{BF}_3$  molecule in the vacuum, respectively. The more negative the  $E_b$  is, the stronger the bond between B-N.

## 2. Figures

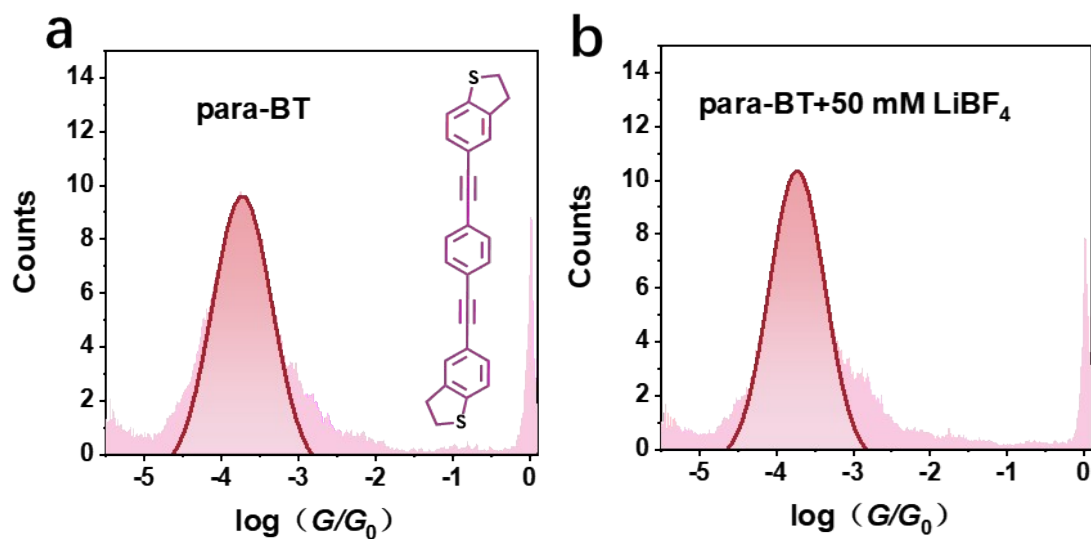


**Figure S1.** (a) 1D conductance histograms obtained in PC solution of 0.1 mM 1,4-bis((2,3-dihydrobenzo[b]thiophen-5-yl)ethynyl). (b) 0.1 mM 1,4-bis((2,3-dihydrobenzo[b]thiophen-5-yl)ethynyl) + 50 mM LiBF<sub>4</sub>. The counts are normalized by the numbers of conductance curves used.

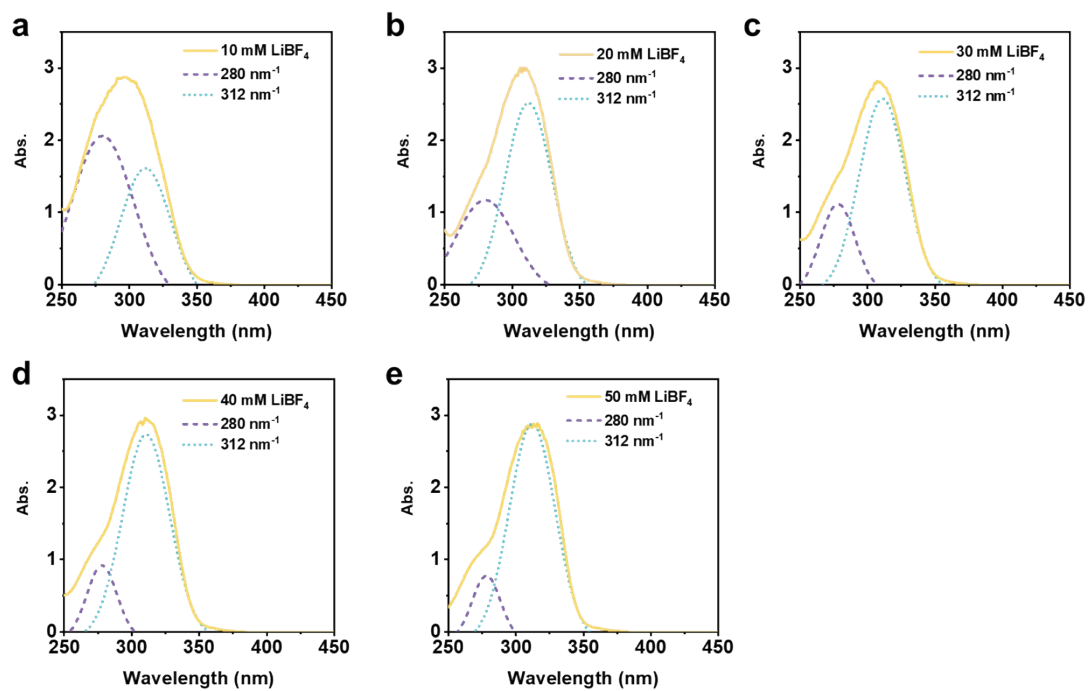


**Figure S2.** Gaussian fitting of UV-vis absorption peaks at different concentrations of (a) 10 mM, (b) 20 mM, (c) 30 mM, (d) 40 mM and 50 mM  $\text{LiBF}_4$ .

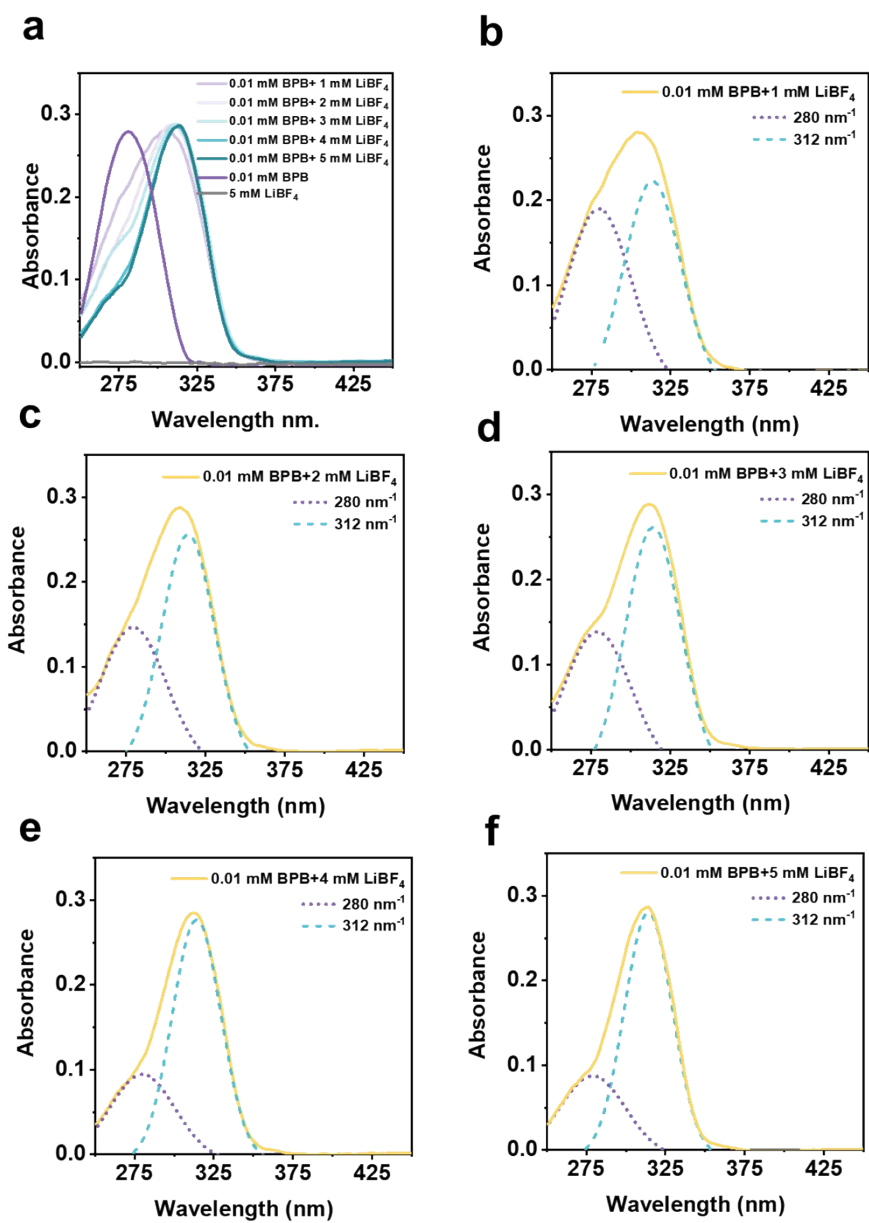


**Figure S3.** (a) Test of UV absorption after ten-fold dilution of the sample. Gaussian fitting of UV-vis absorption peaks at different concentrations of (b) 1 mM, (c) 2 mM, (d) 3 mM, (e) 4 mM and (f) 5 mM LiBF<sub>4</sub>.

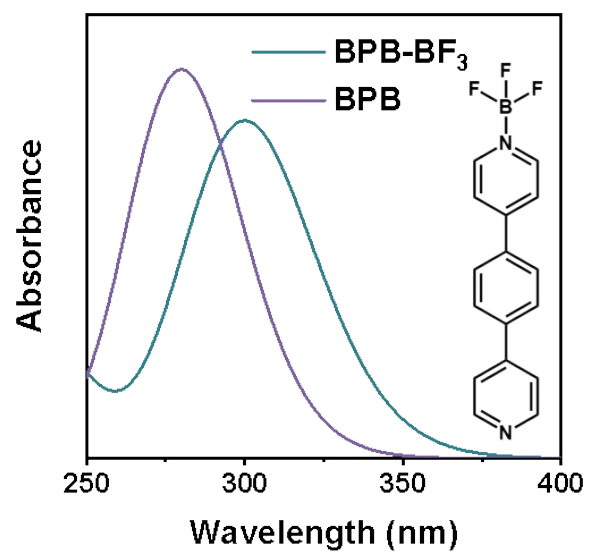


**Figure S4.** UV-vis absorption spectra of BPB and BPB-BF<sub>3</sub> predicted by DFT.

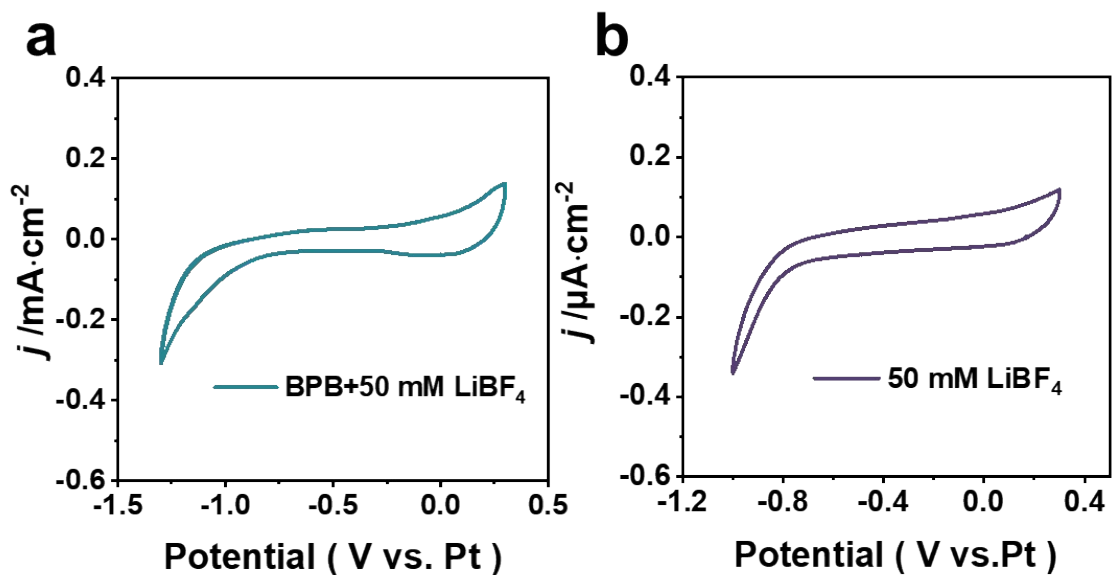


**Figure S5.** CVs of Au(111) in (a) 0.1 mM BPB + 50 mM LiBF<sub>4</sub> solution and (b) 50 mM LiBF<sub>4</sub> solution.

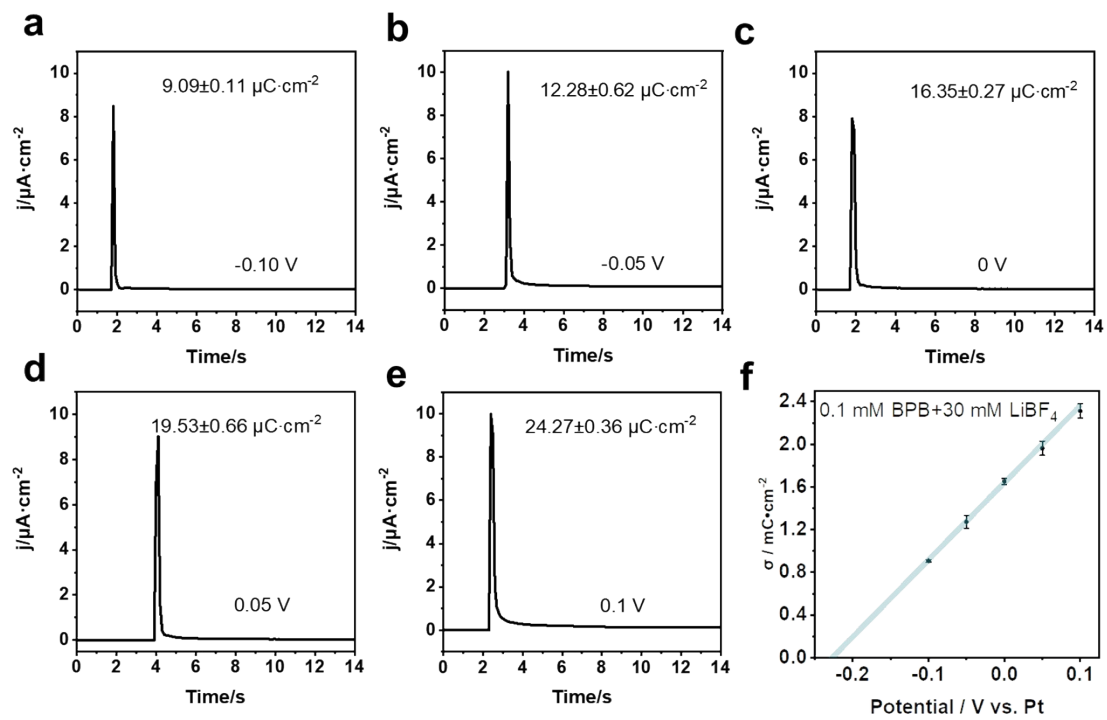


**Figure S6.** Current transients measured during the potentiostatic immersion of a Au(111) electrode in (f) 0.1 mM BPB + 30 mM LiBF<sub>4</sub> with control of different potentials.

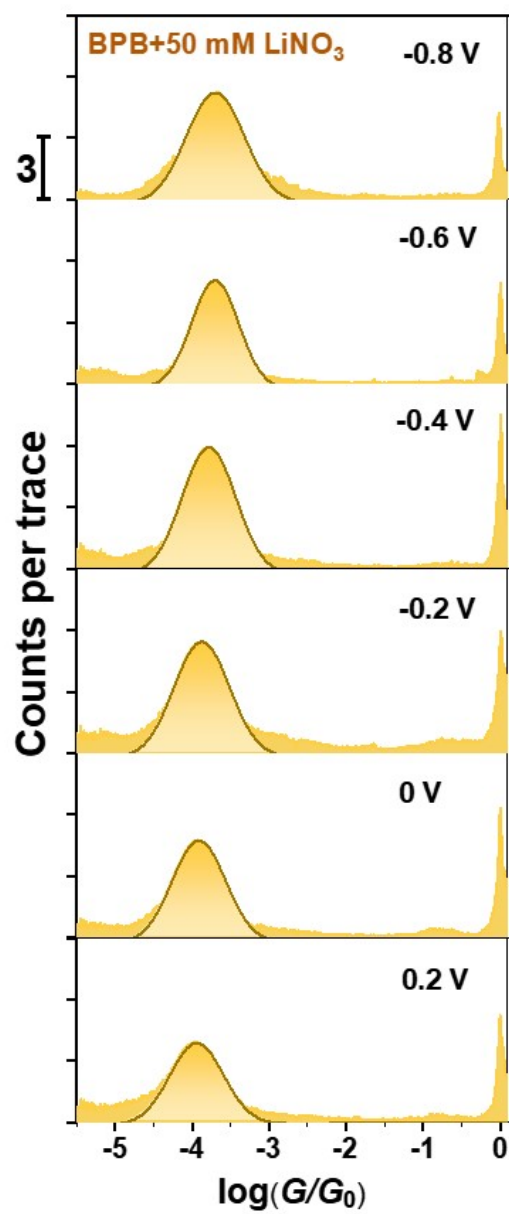


**Figure S7.** The potential dependent 1D conductance histogram of 0.1 mM BPB + 50 mM LiNO<sub>3</sub>.

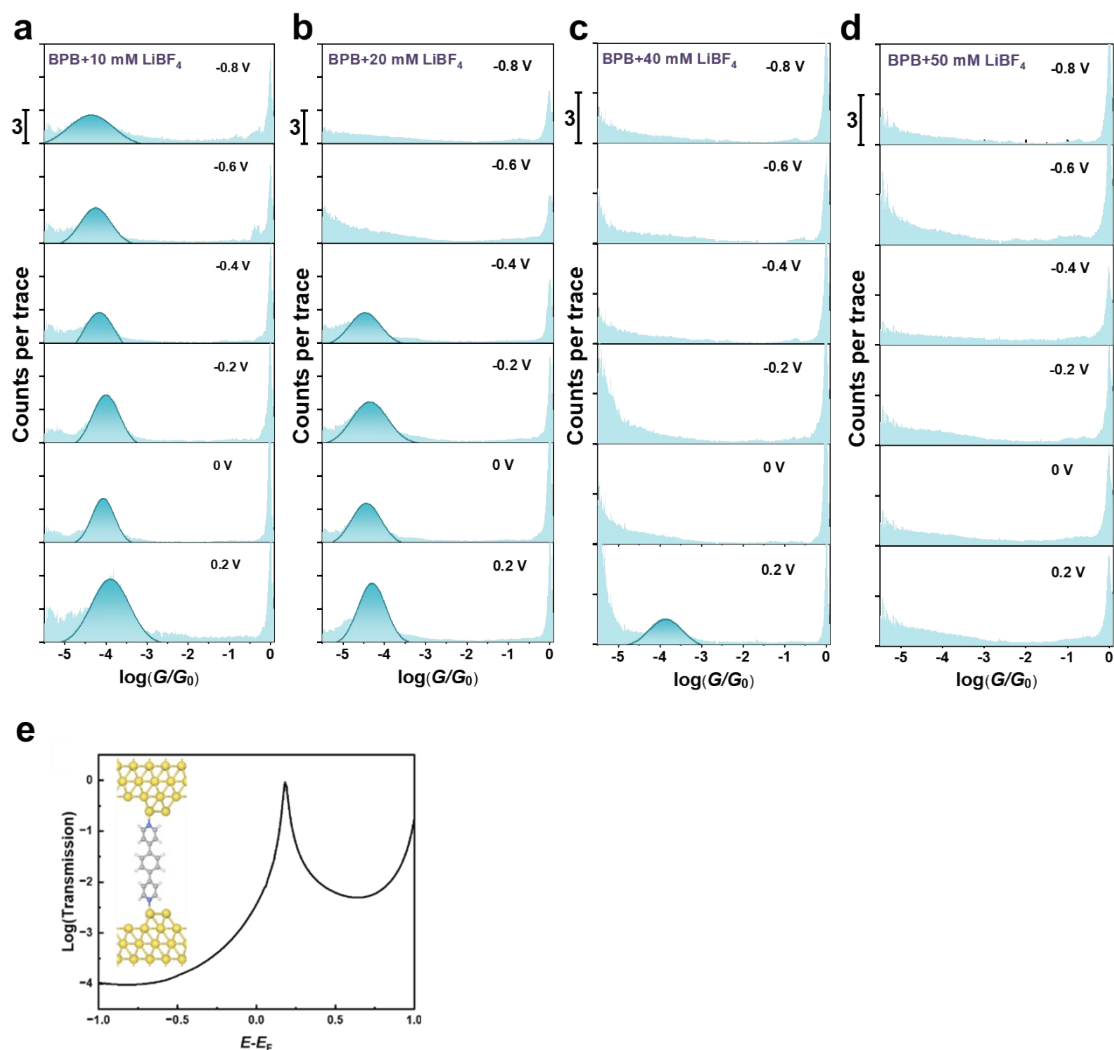


**Figure S8.** The potential dependent 1D conductance histogram of 0.1 mM BPB in (a) 10 mM, (b) 20 mM, (c) 40 mM and (d) 50 mM LiBF<sub>4</sub>. (e) Calculated transmission spectra for Au-BPB-Au.

As shown in Figure S8e, the calculated transmission spectrum shows the LUMO of BPB is closer to Fermi level ( $E_F$ ), corresponding conductance value is dominated by LUMO, consistent with previous reports of pyridine-linked molecular junction. Therefore, the conductance will become larger when decreasing the applied potential to make  $E_F$  close to the LUMO. Meanwhile, we observed the conductance of BPB molecular junctions in LiNO<sub>3</sub> solution slightly become larger when changing the  $E_{\text{substrate}}$  from 0.2 V to -0.8 V (Figure S7). But the conductance of BPB molecular junctions in LiBF<sub>4</sub> solution fluctuates slightly, which might arise from the presence of BF<sub>3</sub> and formation of BPB-BF<sub>3</sub> adduct than can change the surface

coverage and adoption geometries of BPB.

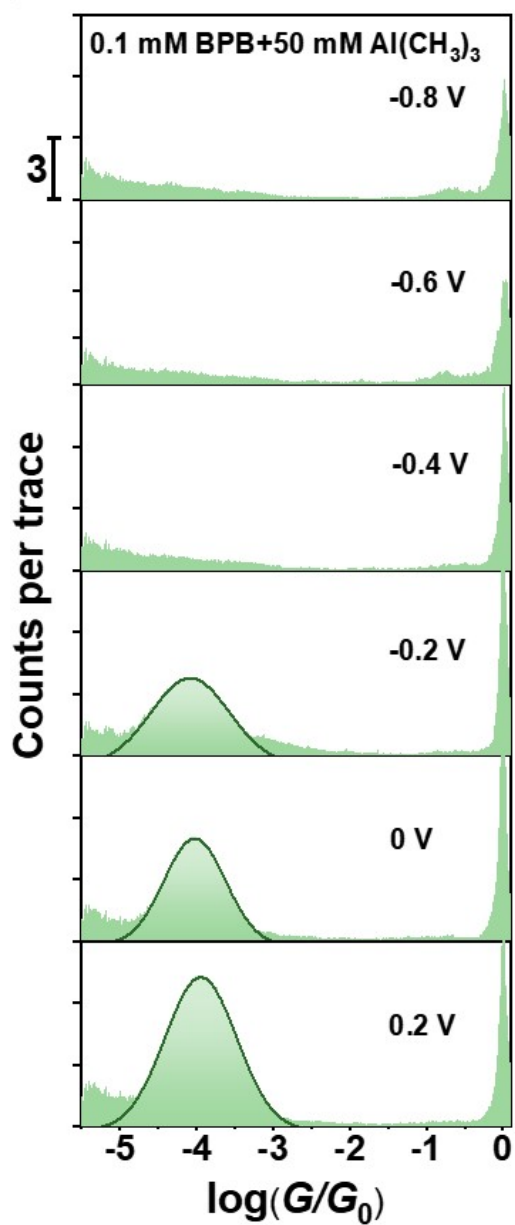


**Figure S9.** The potential dependent 1D conductance histogram of 0.1 mM BPB + 50 mM  $\text{Al}(\text{CH}_3)_3$ .

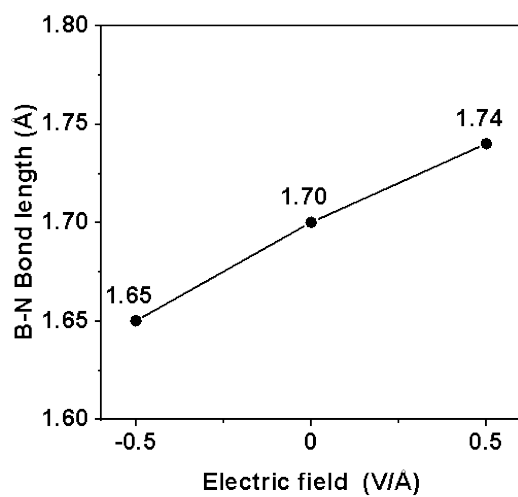


**Figure S10.** B–N length under various electric fields.

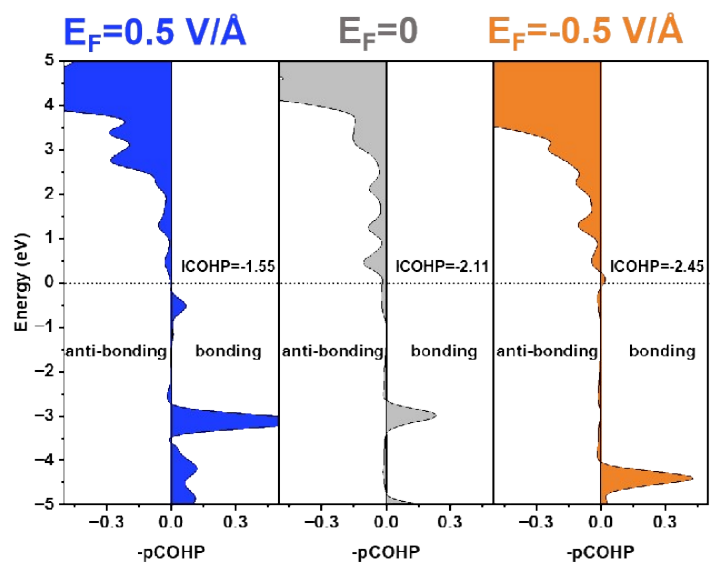


**Figure S11.** The COHP diagrams for B–N bond in BPB on Au(111) with various electric field.

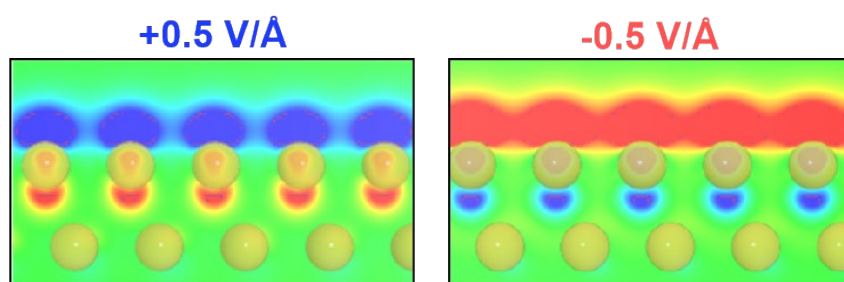


**Figure S12.** 2D slice of electron density difference diagram ( $\Delta\rho = \rho_{(0.5/-0.5)} - \rho_{(0)}$ ) for Au(111), red region represents accumulation of electrons while blue one represents depletion.

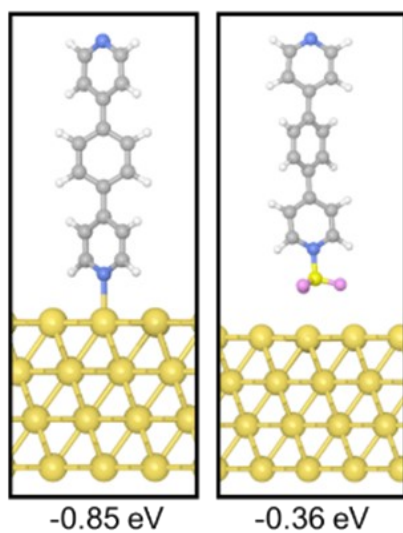


**Figure S13.** Optimized adsorption geometries of BPB and BPB-BF<sub>3</sub> on Au(111), with adsorption energies ( $E_{\text{ads}}$ ) calculated by using  $E_{\text{ads}} = E(\text{Au-BPB}) - E(\text{Au}) - E(\text{BPB})$  and  $E_{\text{ads}} = E(\text{Au-BPB-BF}_3) - E(\text{Au}) - E(\text{BPB-BF}_3)$ , respectively.

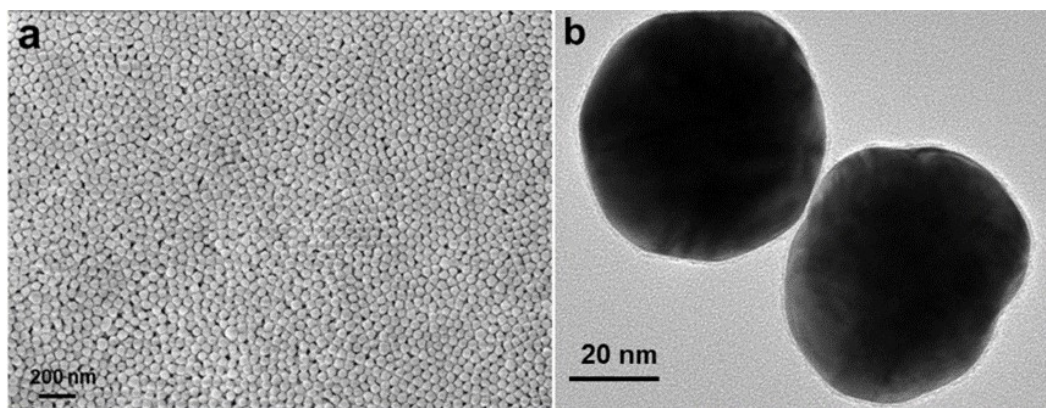


**Figure S14.** (a) SEM and (b) TEM images of 55 nm Au @ ca. 2 nm SiO<sub>2</sub> core-shell nanoparticles.

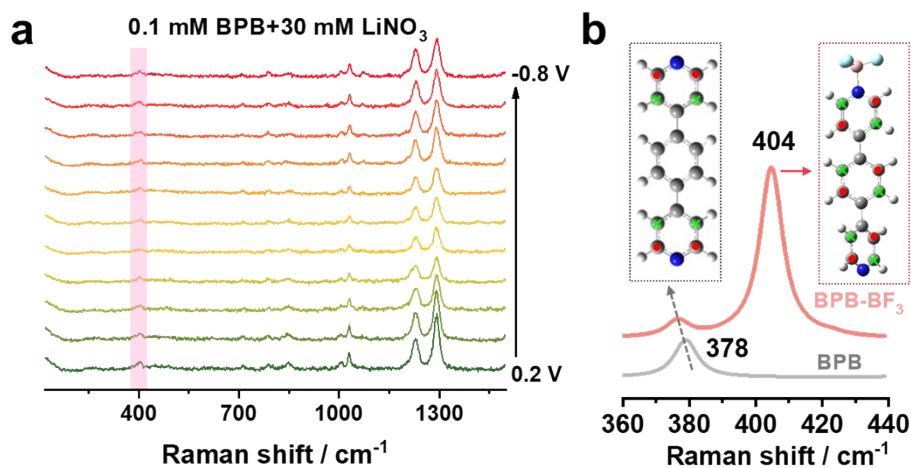


**Figure S15.** (a) Potential-dependent Raman spectra of 0.1 mM BPB + 30 mM LiNO<sub>3</sub>. (b) Theoretical simulated Raman spectra of  $\tau_{cc}$  of BPB, where red dots represent atoms vibrating outward, and green crosses indicate atoms vibrating inward.

The weak peak near 400 cm<sup>-1</sup> in Figure S15a is attributed to the CC out-of-plane twisting ( $\tau_{cc}$ ) vibration of the two pyridine rings, as determined by DFT calculations (Figure S15b). After the formation of the BPB-BF<sub>3</sub> Lewis adduct, the Raman activity of the CC out-of-plane twisting ( $\tau_{cc}$ ) vibration of the benzene ring and pyridine rings is significantly enhanced. Consequently, as shown in Figure 3a, the intensity of the  $\tau_{cc}$  vibration at around 404 cm<sup>-1</sup> markedly increases with the reduction in potential, corresponding to the formation of the BPB-BF<sub>3</sub> Lewis adduct.

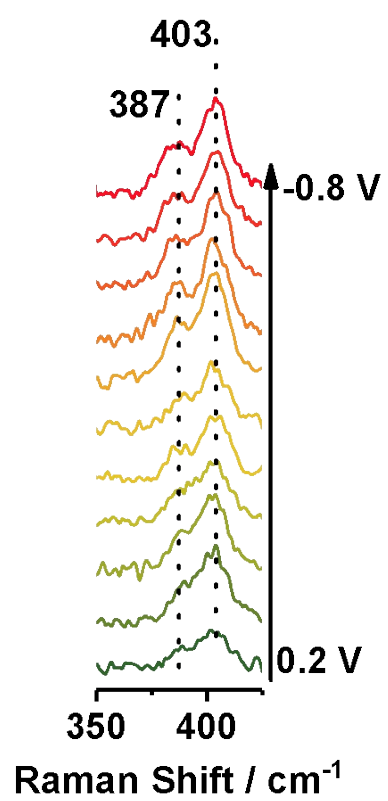


**Figure S16.** Potential-dependent Raman spectra of 0.1 mM BPB + 50 mM LiBF<sub>4</sub>.

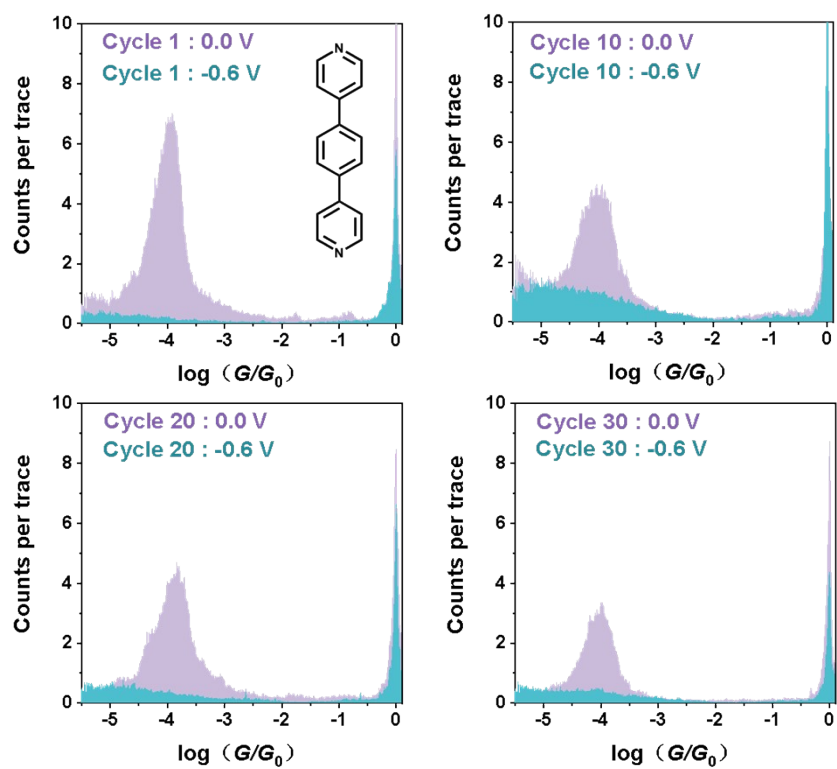


**Figure S17.** 1D conductance histograms of BPB with potential switching between 0 V (purple) to -0.6 V (blue) in 30 cycles.

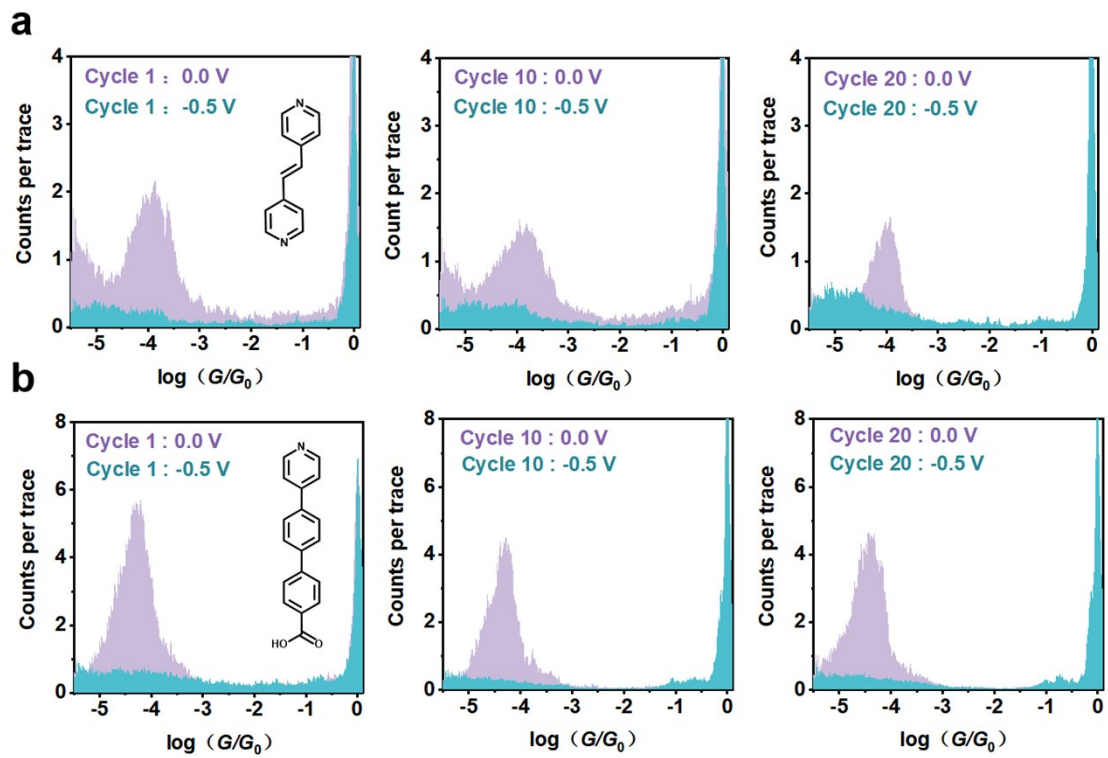


**Figure S18.** 1D conductance histograms of (a) BPY-EE and (b) PBBA with potential switching between 0 V (purple) to -0.5 V (blue) in 20 cycles.

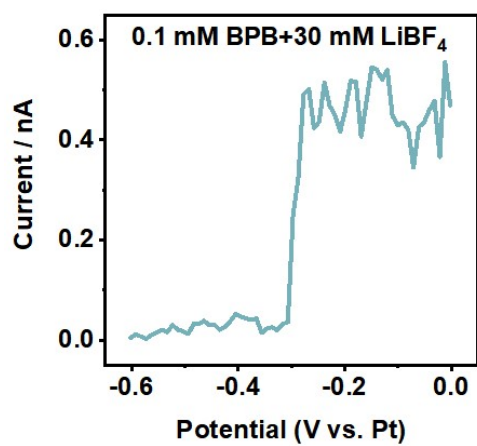


**Figure S19.** A typical I–V curve obtained in 0.1 mM BPB+ 30 mM LiBF<sub>4</sub> with a constant bias of -50 mV by simultaneously sweeping the tip and substrate potentials from 0 V to -0.6 V.

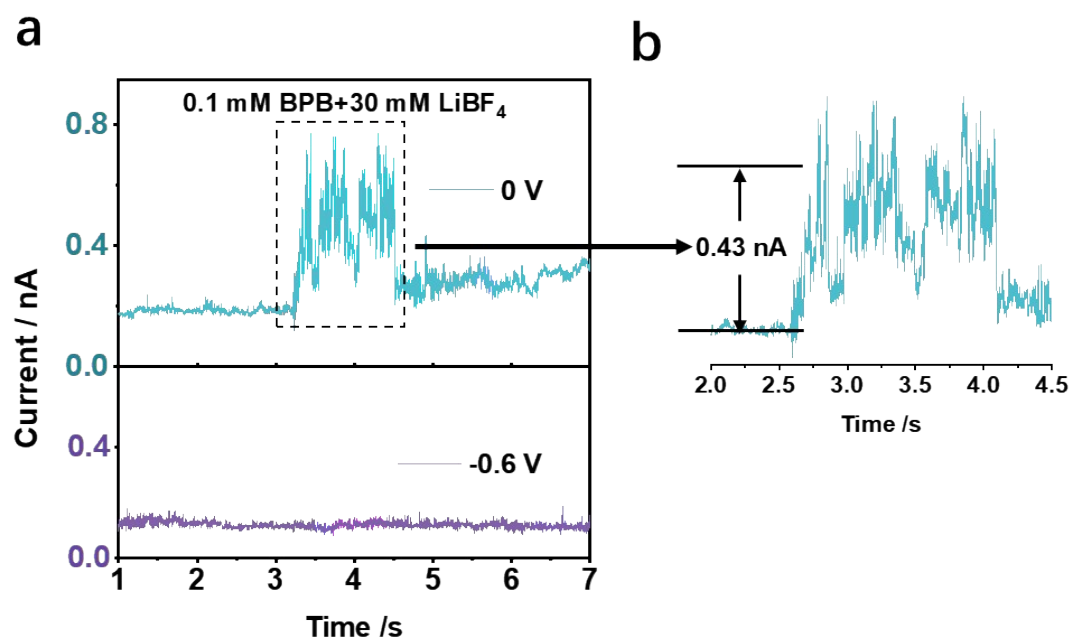


**Figure S20.** (a) Typical I-t traces in 0.1 mM BPB+ 30 mM LiBF<sub>4</sub> solution without feedback loop at the substrate potentials of -0.6 V and 0 V, respectively. Initial tunneling current setpoint is 0.19 nA under a bias voltage of -50 mV. (b) Zoom in I-t trace showing the formation of single-molecule junction formation.

## References

1. Z. Yu, Y. X. Xu, J. Q. Su, P. M. Radjenovic, Y. H. Wang, J. F. Zheng, B. T. Teng, Y. Shao, X. S. Zhou and J. F. Li, Probing Interfacial Electronic Effects on Single-Molecule Adsorption Geometry and Electron Transport at Atomically Flat Surfaces, *Angew. Chem. Int. Ed.*, 2021, **60**, 15452-15458.
2. X. S. Zhou, Y. M. Wei, L. Liu, Z. B. Chen, J. Tang and B. W. Mao, Extending the capability of STM break junction for conductance measurement of atomic-size nanowires: An electrochemical strategy, *Journal of the American Chemical Society*, 2008, **130**, 13228-13230.
3. H. Y. Guo, Q. Wan, Y. J. Jiang, B. Wang, L. Y. Wang, J. F. Zheng, Y. H. Wang, Y. B. Zhang, J. F. Li and X. S. Zhou, Electrochemically Gated Frustrated Lewis Pair Chemistry in Electric Double Layer, *Angew. Chem. Int. Ed.*, 2025, **64**, e202414867.
4. J. F. Li, Y. F. Huang, Y. Ding, Z. L. Yang, S. B. Li, X. S. Zhou, F. R. Fan, W. Zhang, Z. Y. Zhou, D. Y. Wu, B. Ren, Z. L. Wang and Z. Q. Tian, Shell-Isolated Nanoparticle-Enhanced Raman Spectroscopy, *Nature*, 2010, **464**, 392-395.
5. Y. H. Wang, Y. F. Zhou, L. Tong, H. Huang, J. F. Zheng, W. Z. Xie, J. Z. Chen, Y. Shao and X. S. Zhou, Revealing Supramolecular Interactions and Electron Transport in Single Molecular Junctions of Cucurbituril, *Adv. Electron. Mater.*, 2021, **7**, 2100399.
6. M. Frisch, Gaussian 09, Revision D. 01/Gaussian, *Journal*, 2009.
7. G. Kresse and J. Furthmüller, Efficiency of ab-initio total energy calculations for metals and semiconductors using a plane-wave basis set, *Comp. Mater. Sci.*, 1996, **6**, 15-50.
8. P. E. Blöchl, Projector augmented-wave method, *Physical Review B*, 1994, **50**, 17953-17979.
9. J. P. Perdew, K. Burke and M. Ernzerhof, Generalized Gradient Approximation Made Simple, *Physical Review Letters*, 1996, **77**, 3865-3868.
10. S. Grimme, J. Antony, S. Ehrlich and H. Krieg, A consistent and accurate ab initio parametrization of density functional dispersion correction (DFT-D) for the 94 elements H-Pu, *J. Chem. Phys.*, 2010, **132**, 19.
11. H. J. Monkhorst and J. D. Pack, Special points for Brillouin-zone integrations, *Physical Review B*, 1976, **13**, 5188-5192.